ELSEVIER

Ultrasonics 39 (2001) 283–290

Ultrasonics

www.elsevier.nl/locate/ultras

Importance of the near Lamb mode imaging of multilayered composite plates

T. Kundu [a,*], C. Potel [b,c], J.F. de Belleval [b]

[a] *Department of Civil Engineering and Engineering Mechanics, University of Arizona, P.O. Box 210072, Tucson, AZ 85721 0072, USA*
[b] *Laboratoire ROBERVAL, UMR UTC-CNRS, No. 6066, University of Technology of Compiegne, BP 20529, 60205 Compiegne Cedex, France*
[c] *Dept OGP Soissons, IUT de l'Aisne, University Picardie Jules Verne, 02880 Cuffies, France*

Received 1 November 1999; received in revised form 1 November 2000; accepted 1 December 2000

Abstract

In recent years Lamb waves are being used for internal defect detection in multilayered composite plates. Different Lamb modes generate various stress levels in different layers. As a result, all Lamb modes are not equally sensitive to internal defects of various layers. A number of studies have been carried out to identify which Lamb mode is most effective for detecting defects in a specific layer. However, one shortcoming of the Lamb wave inspection technique is that in a symmetrically layered composite plate stress and displacement magnitudes and energy distribution profiles for all Lamb modes are symmetric about the central plane of the plate. As a result, the ability of a Lamb mode to detect defects in a specific layer of the plate is identical to its ability to detect defects in the corresponding layer of mirror symmetry. Hence, from the Lamb wave generated image one cannot distinguish between the defects in these two layers of mirror symmetry. In this paper it is investigated how by fine-tuning the frequency and the striking angle of the incident beam in the neighborhood of a Lamb mode one can separately detect internal defects in layers of mirror symmetry in the upper and lower halves of a plate. © 2001 Elsevier Science B.V. All rights reserved.

Keywords: Lamb waves; Multilayered composite plates

1. Introduction

In this decade several investigators have tried to use Lamb waves for detecting internal defects in laminated composite plates. This is done by scanning the composite plate specimen by two transducers oriented in a defocused pitch-catch position [11,12,14] or a focused pitch-catch position such that the receiver is in the null zone of the reflected beam [4]. Alternatively, the specimen can be scanned by only one transducer that acts both as the transmitter and the receiver to generate and receive leaky Lamb waves [15].

When one wants to use Lamb waves for detecting defects inside a plate, one should first know which Lamb mode to be used for detecting defects at a specific depth of the plate. To this aim Ditri et al. [5] studied the energy distribution inside a plate for different Lamb modes and tried to relate the energy distribution profile to the defect detection capability of the Lamb modes. For the frequency–thickness values ($fd = 4.78$ and 6.35 MHz/mm) considered during the inspection they found that both symmetric (S_2) and antisymmetric (A_1) modes have maximum energy flow rate at the central plane of the plate. Hence, these modes should be more sensitive to defects at the central plane than those near the surface. However, it was later shown by Maslov and Kundu [14] that symmetric and antisymmetric modes are not equally sensitive to the defects located at the central plane of the plate. Energy distribution curves can be used for correctly predicting the detectability of the vertical cracks in a plate as Ditri et al. [5] did. However, this approach is of little use to predict which modes are sensitive to horizontal cracks or delamination defects. For such predictions one needs to compute the stress distribution profiles inside the plate. If a defect releases a specific component of stress then the Lamb mode, that produces maximum level of that stress component at the defect position, should be most sensitive to that defect. Information on the internal variation of other stress

---

[*] Corresponding author. Tel.: +1-602-621-6573; fax: +1-602-621-2550.
E-mail address: tkundu@u.arizona.edu (T. Kundu).

PII: S0041-624X(01)00052-X

components that are not released by the defect is not of interest since both defective and defect-free specimens should produce the same levels of those stress components.

The importance of computing the internal particle displacement and stress variation in a specimen for detecting internal defects by Lamb waves and other ultrasonic techniques have been recognized by many investigators [1,16,22]. Maslov and Kundu [14] and Yang and Kundu [22] computed the internal stress field variation in a five-layer and a 12-layer composite plate respectively, for different Lamb modes. They have experimentally shown that the Lamb mode which produces the maximum stress level in a specific layer is most effective in detecting defects in that layer.

2. Motivation

In spite of many advantages of the Lamb wave technique for detecting internal defects in a composite plate one major disadvantage of this technique is its inability to distinguish between defects in layers of mirror symmetry. If one puts a multilayered composite beam or plate in a three- or four-point bending machine then the lower half of the plate is subjected to tension and the upper half to the compression. Naturally defects generated due to this loading in the lower and upper halves of the plate are different. If the Lamb wave scanning technique cannot distinguish between the defects in layers of mirror symmetry then this technique is of little use to study the crack initiation and propagation behavior in composite plates subjected to non-symmetric loading.

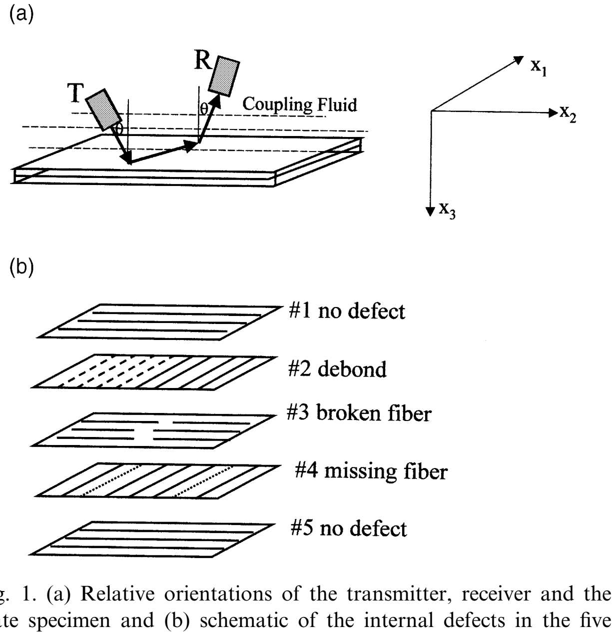

Fig. 1. (a) Relative orientations of the transmitter, receiver and the plate specimen and (b) schematic of the internal defects in the five layers of the composite plate specimen.

This research was undertaken to modify the current Lamb wave scanning technique so that identical defects in layers of mirror symmetry can be discriminated from one another. To this aim internal displacement and stress fields in a multilayered composite plate, having layers of mirror symmetry, are computed. Kundu et al. [12] and Maslov and Kundu [14] scanned a five-layer composite plate by different Lamb modes. Fig. 1 shows the pitch-catch arrangement of the transmitter (T) and the receiver (R) for scanning this specimen. The specimen was scanned by moving the transmitter and the receiver simultaneously in the x_1–x_2 plane without altering the relative positions of T and R. The Lamb wave propagation direction is the x_1 direction. This specimen is considered here for theoretically computing the internal stress and displacement profiles.

3. Specimen description

The specimen is a five-layer metal matrix composite plate of dimension $80 \times 33 \times 1.97$ mm^3. Five layers or plies of SCS-6 fibers in Ti–6Al–4V matrix are oriented in 90° and 0° directions in alternate layers. SCS is a copyrighted/registered name by the fiber manufacturer, the Textron Inc. This fiber has a carbon core of about 25 μm diameter, two concentric layers of silicon carbide (SiC) surround the carbon core and finally two very thin (a few microns thick) layers of carbon coating are placed on the outside. The overall fiber diameter is about 152 μm. The fibers in the top, middle and bottom layers are oriented in the x_2 direction or along the length of the plate; the other two plies are in the x_1 direction or along the width of the plate (see Fig. 1). The composite was made by the foil-fiber-foil technique. The internal flaws, shown in Fig. 1, were intentionally introduced in the plate during the fabrication process. The first (top) and the fifth (bottom) layers of fibers did not have any flaw. The left part of the second layer fibers was coated with boron nitride to impede the formation of good bonding between the fibers and the matrix as schematically shown in Fig. 1. The fibers in the third layer were intentionally broken near the middle. The fourth layer had two areas of missing fibers, on the left side five fibers and on the right side 10 fibers were removed. Photographs of the third and fourth layers are shown in Fig. 2. These photographs were taken before fabricating the specimen. Broken and missing fiber zones can be clearly seen in these photographs.

Fig. 1 shows how the specimen was scanned by propagating Lamb waves in the direction normal to the fibers of layers 1, 3 and 5 and parallel to the fibers of layers 2 and 4. Before investigating the images generated by Lamb waves we first scanned the specimen by the normal incidence C-scan technique. The C-scan images are shown in Fig. 3. Three images of Fig. 3 are generated

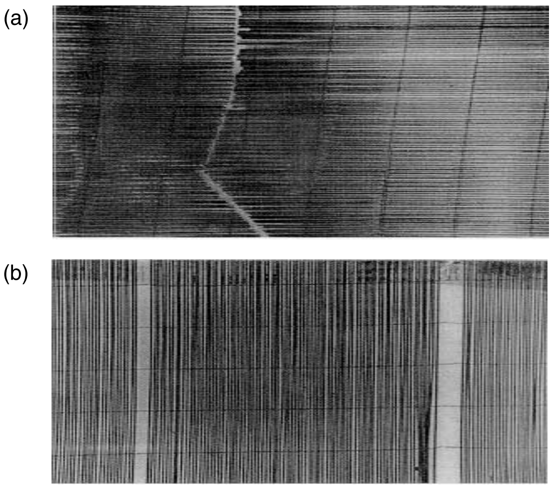

Fig. 2. Photograph of (a) the broken fibers of the third layer and (b) missing fibers of the fourth layer, taken before fabricating the specimen [12].

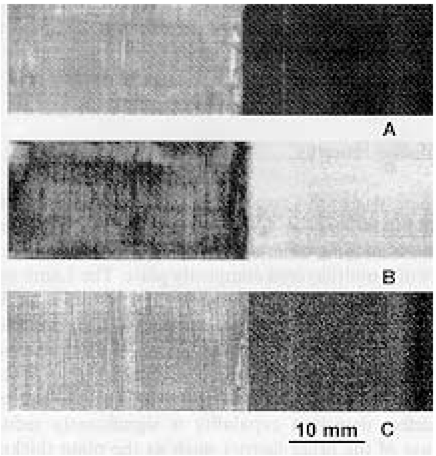

Fig. 3. Conventional C-scan images generated by 10 MHz (top and middle) and 75 MHz (bottom) focused transducers used in the pulse-echo mode. The back surface echo is omitted for constructing the top and bottom images and it is considered for the middle image. Broken fibers and missing fibers can be faintly seen in some of these images [12].

by 10 MHz (top and middle) and 75 MHz (bottom) focused transducers used in the pulse-echo mode. The transducer axis is positioned normal to the plate specimen. For the top and bottom images the gate position is such that the reflected signals from the middle of the layer are received and the back surface echo is omitted, hence the internal defects should clearly be seen in these two images; for the middle image the back surface is recorded. In all these three images the debond can be clearly seen. The missing and broken fibers can be faintly seen in some images. However, delamination is the only defect that can be clearly seen in all three images.

For understanding and analyzing the Lamb wave generated images one should compute the internal stress and displacement profiles when Lamb waves propagate in the direction normal to the fibers of layers 1, 3 and 5. In other words, the fiber orientation relative to the Lamb wave propagation direction is 90° for layers 1, 3 and 5, and 0° for layers 2 and 4. During the experiment the specimen was immersed in water. That is why the theoretical stress and displacement profiles are computed for the composite plate immersed in water for leaky Lamb wave propagation.

4. Numerical computation

A number of investigators have studied the mechanics of elastic wave propagation in multilayered anisotropic solids [3,7,13,16,18–20,22]. Since this theory is already available in the literature, our purpose here is not to present the theory again but to use it to compute the internal stress and displacement fields to get an insight how to use Lamb modes most effectively to detect internal defects in multilayered composite plates. Yang and Kundu [22] studied the leaky Lamb wave propagation in multilayered composite plates. Results presented below are obtained following their technique for the composite plate immersed in water.

For computing internal stresses and displacements in a multilayered plate one needs to know all elastic constants of individual layers. However, the authors did not know the five independent elastic constants of individual layers of hexagonal symmetry and could not measure those easily. Only the density (4.1 gm/cm^3) of the plate could be measured without any difficulty. P-wave speed (1.49 km/s) and density (1 gm/cm^3) of the coupling fluid (water) were also known to the authors.

Huang et al. [6] gave elastic properties of titanium (Ti) and SiC for SCS-6 fiber reinforced titanium matrix. These properties are listed in Table 1.

Table 1
Elastic properties of Ti and SiC

Material	Young's Modulus (E, GPa)	Poisson's ratio (ν)	Lame's first constant (λ, GPa)	Shear modulus (G, GPa)	Density (ρ, gm/cm^3)
Ti[a]	121.6	0.35	103.3	45.1	5.4
Ti[b]	96.5	–	55.9	37.1	4.5
SiC[a]	415.0	0.17	91.4	177.4	3.2
SiC[b]	431.0	–	176	172.0	3.2

[a] Ref. [6].

[b] Ref. [21].

From the above table the stress–strain relation for Ti and SiC can be written in the following form. In the constitutive matrix (or [C] matrix) a range is given for each element. This range is obtained from the two sets of values of the elastic constants given in Table 1.

Stress–strain relation for Ti,

$$\begin{Bmatrix} \sigma_{11} \\ \sigma_{22} \\ \sigma_{33} \\ \sigma_{23} \\ \sigma_{31} \\ \sigma_{12} \end{Bmatrix} = \begin{bmatrix} 130.1\text{–}193.5 & 55.9\text{–}103.3 & 55.9\text{–}103.3 & 0 & 0 & 0 \\ & 130.1\text{–}193.3 & 55.9\text{–}103.3 & 0 & 0 & 0 \\ & & 130.1\text{–}193.3 & 0 & 0 & 0 \\ & & & 37.1\text{–}45.1 & 0 & 0 \\ & & & & 37.1\text{–}45.1 & 0 \\ & & & & & 37.1\text{–}45.1 \end{bmatrix} \begin{Bmatrix} \varepsilon_{11} \\ \varepsilon_{22} \\ \varepsilon_{33} \\ 2\varepsilon_{23} \\ 2\varepsilon_{31} \\ 2\varepsilon_{12} \end{Bmatrix} \tag{1}$$

and for SiC,

$$\begin{Bmatrix} \sigma_{11} \\ \sigma_{22} \\ \sigma_{33} \\ \sigma_{23} \\ \sigma_{31} \\ \sigma_{12} \end{Bmatrix} = \begin{bmatrix} 446\text{–}520 & 91.4\text{–}176 & 91.4\text{–}176 & 0 & 0 & 0 \\ & 446\text{–}520 & 91.4\text{–}176 & 0 & 0 & 0 \\ & & 446\text{–}520 & 0 & 0 & 0 \\ & & & 172\text{–}177.4 & 0 & 0 \\ & & & & 172\text{–}177.4 & 0 \\ & & & & & 172\text{–}177.4 \end{bmatrix} \begin{Bmatrix} \varepsilon_{11} \\ \varepsilon_{22} \\ \varepsilon_{33} \\ 2\varepsilon_{23} \\ 2\varepsilon_{31} \\ 2\varepsilon_{12} \end{Bmatrix} \tag{2}$$

The constitutive matrices for both Ti and SiC in Eqs. (1) and (2) are isotropic and have two independent elastic constants. However, SiC fiber reinforced Ti matrix composite has hexagonal symmetry. Hence, the [C] matrix for the composite will be anisotropic and will have five independent elastic constants. Experimental values of phase velocity for different Lamb modes at various frequencies, as obtained by Kundu et al. [12] are shown by open triangles in Fig. 4. A total of twenty triangles are shown in this figure.

The [C] matrix of the individual layers of the five-layer composite plate are obtained by the trial and error method by matching the theoretical dispersion curves with the experimental points. After a number of trials the following stress–strain relation gave the best fit between the theoretical curves and the experimental points,

$$\begin{Bmatrix} \sigma_{11} \\ \sigma_{22} \\ \sigma_{33} \\ \sigma_{23} \\ \sigma_{31} \\ \sigma_{12} \end{Bmatrix} = \begin{bmatrix} 325 & 103 & 103 & 0 & 0 & 0 \\ & 194 & 92 & 0 & 0 & 0 \\ & & 194 & 0 & 0 & 0 \\ & & & 51 & 0 & 0 \\ & & & & 100 & 0 \\ & & & & & 100 \end{bmatrix} \begin{Bmatrix} \varepsilon_{11} \\ \varepsilon_{22} \\ \varepsilon_{33} \\ 2\varepsilon_{23} \\ 2\varepsilon_{31} \\ 2\varepsilon_{12} \end{Bmatrix} \tag{3}$$

where x_1 is the fiber direction, elastic constants are given in GPa. Note that $c_{44} = (c_{22} - c_{23})/2$. Theoretical leaky Lamb wave dispersion curves for the five-layer composite plate of 1.97 mm total thickness are shown in Fig. 4 by black diamond symbols connected by continuous lines. These are computed with the individual layer properties given in Eq. (3) and Lamb waves propagating normal to the fiber direction of the top layer (see Fig. 1). Lamb modes are numbered from 1 to 7 from left (low frequency) to right (high frequency). It should be noted here that the matching between the experimental values and the theoretical dispersion curve is good for the five modes (14 out of the 17 experimental values for these five modes almost coincide with the theoretical curve). The sixth and seventh modes did not match that well with the theoretical curves. This matching can be further improved by adjusting the elastic properties of the layers by more trial and error iterations or by implementing sophisticated optimization schemes such as the simplex algorithm [2,7–10,17]. After obtaining the elastic properties with reasonable accuracy our next objective is to modify the conventional Lamb wave scanning technique such that the modified technique can discriminate between the defects in layers of mirror symmetry in the multilayered composite plate. It should be noted here that, as expected, the density and all elastic constants of Eq. (3) are in between the corresponding values for Ti and SiC given in Eqs. (1) and (2). It gives an additional confidence on the material constants given in Eq. (3).

Stress profiles are computed for different frequency–phase velocity combinations on and around the second and third Lamb modes. These frequency–phase velocity combinations for which stress profiles have been computed are denoted by a_j, b_j, c_j and d_j ($j = 1$ and 2) and shown by eight crosses in Fig. 4. The plots are obtained for a plane longitudinal wave of a given frequency striking the composite plate at a specified angle. The phase velocity is obtained from the incident angle using

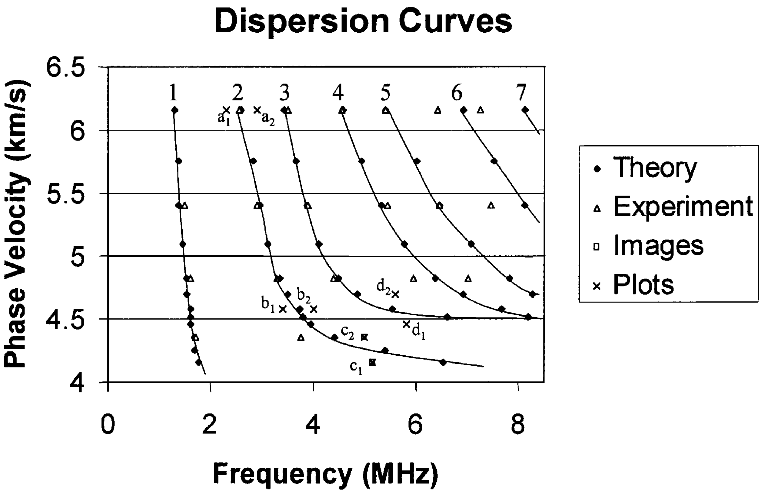

Fig. 4. Numerically computed dispersion curves (diamond symbols connected by continuous lines). Twenty experimental points are shown by triangular symbols. Stress plots of Figs. 5, 6 and 8 are generated for eight different frequency–phase velocity combinations (a_j, b_j, c_j and d_j, $j = 1$ and 2); those points are shown by square markers. Cross markers (points c_1 and c_2) show the frequency–phase velocity combinations used for generating the two images of Fig. 6. The seven modes are numbered from 1 to 7.

the Snell's law (Eq. (4)). If the phase velocity frequency combination is such that it is near a leaky Lamb mode but does not coincide exactly with the dispersion curve then the stress and displacement components would differ from those for the leaky Lamb wave propagation. It should be mentioned here that for the stress field computations near Lamb modes the contributions of incident, reflected and transmitted waves in the upper and lower fluid half spaces must be considered. The incident angle should be set such that the phase velocity computed from the Snell's law becomes close to a Lamb mode phase velocity. Because of the presence of the incident, reflected and transmitted signals the normal stress components at the top and bottom surfaces of the plate will not have same values. However, in absence of the incident plane wave in the fluid only pure Lamb modes can propagate through the plate and normal stress components at the top and bottom surfaces become equal.

Images of the composite plate have been generated for two different frequency–phase velocity combinations (c_1 and c_2); those two points are marked by two squares in Fig. 4.

Figs. 5 and 6 show the computed stress profiles along the thickness or depth of the plate for six frequency–phase velocity combinations, two pairs (a_j and b_j) near the second mode and one pair (d_j) near the third mode. Fig. 5 shows the shear stress (σ_{13}) variations along the depth of the plate. Fig. 6 shows the normal stress variations (σ_{33} in the left column and σ_{11} in the right column). The phase velocity (V_{ph}) and the incident angle (θ) are related by the Snell's law,

$$V_{\mathrm{ph}} = \frac{V_{\mathrm{f}}}{\sin\theta} \tag{4}$$

V_{f} is the longitudinal wave speed in the coupling fluid. For water it is 1.49 km/s.

The horizontal axes of Figs. 5 and 6 show the depth along the plate thickness (or x_3) direction (see Fig. 1a) varying from zero (top of the plate) to 1.97 mm (bottom of the plate). Since the plate has five layers of identical thickness the layer interfaces are located at 0.394, 0.788, 1.182 and 1.576 mm. In Figs. 5 and 6 the horizontal axis is marked at 0.4, 0.8, 1.2 and 1.6 mm, very close to the layer interface positions. In each plot of Figs. 5 and 6 two curves are shown. Dotted lines correspond to the frequency–phase velocity combinations that are located slightly below or left of the Lamb modes and the continuous lines correspond to the points slightly above or right of the Lamb modes. The curves in Figs. 5 and 6 are marked as SIJ-θ, F, α_j where θ is the angle of incidence in degree, F is the signal frequency in MHz, α_j identifies the point (a_j, b_j, c_j or d_j) of Fig. 4, and SIJ stands for S13 for shear stress (σ_{13}), and S33 or S11 for normal stresses (σ_{33} or σ_{11}). Note that the curves are not symmetric about the central plane of the plate. Hence, these near Lamb modes should be able to distinguish defects in a layer from similar defects in the layer of mirror symmetry.

It should be noted here that the continuous curves give relatively higher values in the lower half of the plate. σ_{13} and σ_{11} in the lower half of the plate (in the fourth layer) is much larger than that in the second layer for frequency–phase velocity combinations corresponding to the points a_2 and b_2 of Fig. 4. On the other hand, for points a_1 and b_1 the first and second layer responses are larger than the fourth and fifth layer responses. This difference is less prominent for σ_{33}. This general trend is true for points d_1 and d_2 also. However, for the continuous curves the differences in σ_{13} (or σ_{11}) in the upper

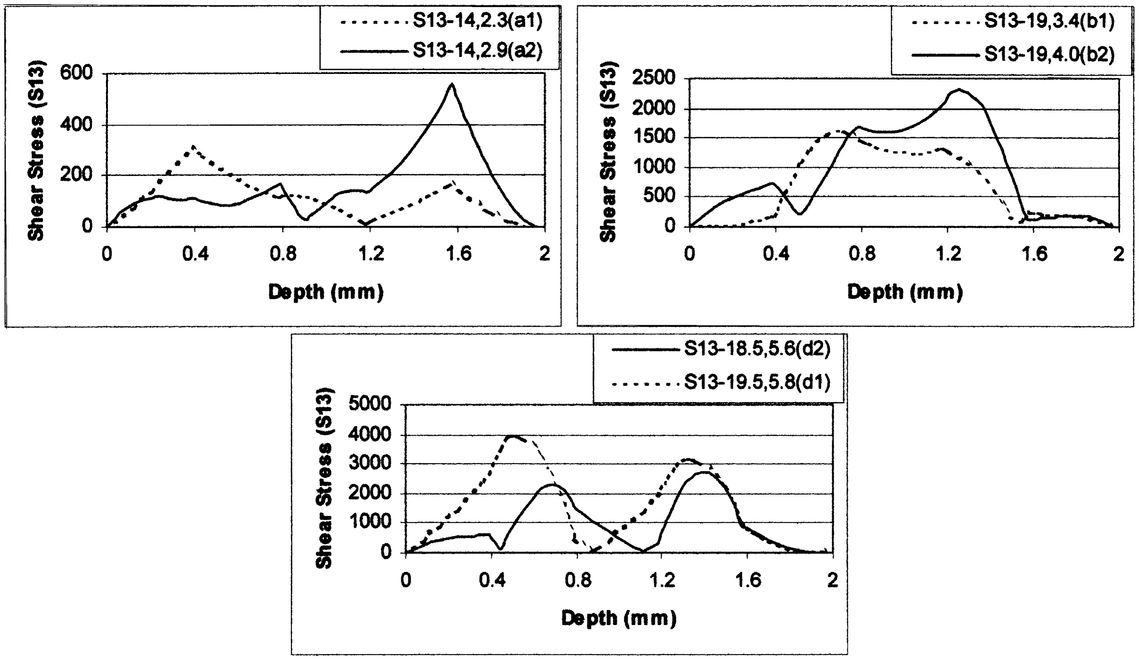

Fig. 5. Shear stress variations inside the composite plate near second (top figures) and third (bottom figure) Lamb modes. Dotted lines have been generated for the frequency–phase velocity combinations denoted by points a_1, b_1 and d_1 in Fig. 4. Points a_2, b_2 and d_2 of Fig. 4 generate the continuous curves.

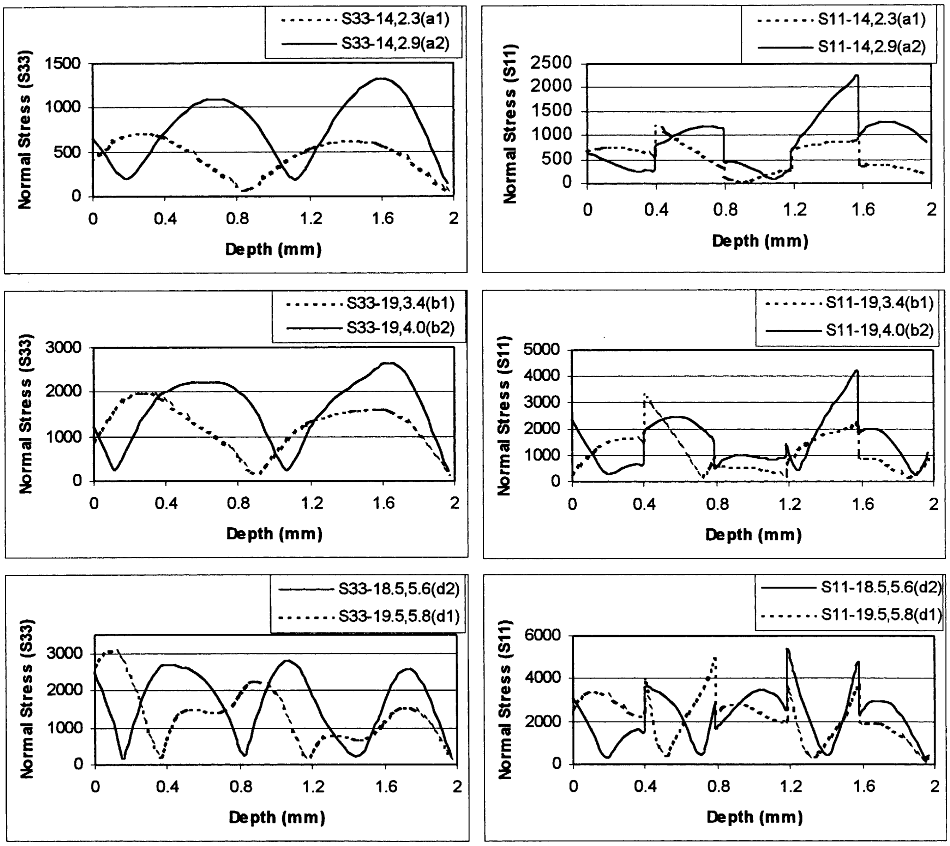

Fig. 6. Normal stress variations inside the composite plate near second and third Lamb modes. Dotted lines have been generated for the frequency–phase velocity combinations denoted by points a_1, b_1 and d_1 in Fig. 4. Points a_2, b_2 and d_2 of Fig. 4 generate the continuous curves. σ_{33} and σ_{11} are shown in the left and right columns, respectively.

and lower halves of the plate for points d_j are not as much as those for points a_j and b_j. Hence, results in Figs. 5 and 6 can be summarized as

1. Stress fields in the neighborhood of a Lamb mode are not symmetric with respect to the central plane of symmetry of the plate.
2. If moving in one direction relative to the Lamb mode causes the stresses to grow in the upper half of the plate then an opposite direction movement will cause the stresses to grow in the lower half of the plate.
3. The percentage difference in the stress values between two layers of mirror symmetry in the lower and upper halves of the plate is not same for all stress components.
4. The percentage difference in the stress values between two layers of mirror symmetry in the neighborhood of a Lamb mode varies from one Lamb mode to another.

Is this difference of stresses sufficient to distinguish between the defects in the upper and lower halves of the plate? To answer this question two images of the specimen have been generated with the frequency–phase velocity combinations corresponding to points c_1 and c_2 of Fig. 4. It should be mentioned here that point c_1 corresponds to the 21° incident angle and 5.15 MHz signal frequency, and for point c_2 the incident angle is 20° and the signal frequency is 5 MHz. A laboratory-made ultrasonic scanner was used for generating the ultrasonic images. A broad band Panametrics transducer (0.5 in. diameter) was excited using Matec 310 gated amplifier with tone-burst signals from the Wavetek function generator. The reflected signal was received by a Matec receiver and was digitized by a GAGE 40 MHz data acquisition board, and then the received signal was analyzed. The computer program computed either the peak to peak or the average amplitude of the signal in a given time window and then plotted it in a gray scale with respect to the horizontal (x_1, x_2) position of the transducers. The window was set near the first arrival time of the signal thus reflections from the plate boundary were avoided.

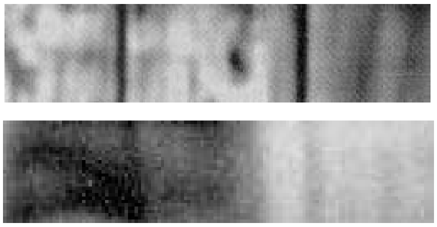

Fig. 7. Two images of the five layer composite plate specimen generated by two different frequency–phase velocity combinations, shown by points c_1 and c_2 in Fig. 4. The top image has been generated by 5.0 MHz signal incident at 20° (point c_2) and the bottom image has been produced by 5.15 MHz signal incident at 21° (point c_1) [12,14].

Generated images are shown in Fig. 7. The 5 MHz signal, incident at 20°, clearly shows the missing fiber defects of the fourth layer and the 5.15 MHz signal, incident at 20°, shows the delamination defect (darker region) of the second layer. It also faintly shows the missing fibers of the fourth layer.

Delamination and missing fibers reduce the shear stress carrying capacity at the defect position. Note that the compressive normal stress σ_{33} can be present at the defect position from the non-vanishing contact pressure. Hence, a study of the σ_{13} profile is critical for predicting the sensitivity of the propagating waves to delamination and missing fiber type defects. σ_{13} profiles for points c_1 and c_2 of Fig. 4 are shown in Fig. 8. It should be noted here that for the 5 MHz signal σ_{13} is very small in the second layer and it is maximum in the fourth layer. That is why in Fig. 7 we see that the image generated by the 5 MHz signal clearly shows the missing fiber defects of the fourth layer and completely ignores the delamination defect of the second layer. On the other hand for the 5.15 MHz signal (dotted line of Fig. 8) the shear stress is maximum in the second layer and very small in the fourth layer. This explains why the image generated by the 5.15 MHz signal shows the delamination defect

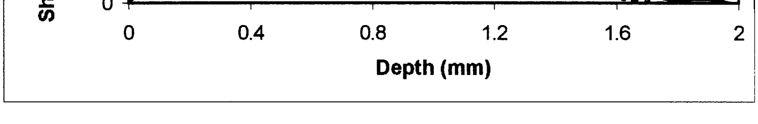

Fig. 8. Shear stress variations inside the composite plate for frequency–phase velocity combinations, denoted by points c_1 (- - -) and c_2 (—) in Fig. 4. Corresponding ultrasonic images are shown in Fig. 7.

(darker region) of the second layer while the missing fiber defect of the fourth layer is not so clear.

Advantage of the near Lamb mode imaging is clearly demonstrated here. In the conventional C-scan image (Fig. 3) the delamination defect guards the missing fiber defects, but in the near Lamb wave image (Fig. 7) the delamination defect does not have any effect on the missing fiber defects when the right frequency–angle combination is selected.

5. Concluding remarks

In this paper it is shown that one can image a specific layer in the lower half (or upper half) of a multilayered composite plate separately from its layer of mirror symmetry by near Lamb mode imaging. In other words, defects in two layers of mirror symmetry can be imaged separately by simply fine tuning the incident angle and/or the signal frequency in the neighborhood of a Lamb mode. The incident angle and the signal frequency should be such that they are close to a Lamb mode but not exactly on the Lamb mode. The Lamb modes investigated here show that the nature of asymmetry in the stress field changes in opposite directions as the point moves from one side of a Lamb mode curve to the other side. In other words, if a point on the left side of a dispersion curve gives larger stress in the upper half of the plate, a point on the right side of the curve gives larger stress in the lower half of the plate. For two consecutive modes it changes, i.e. if a point located slightly left of mode N gives larger stress in the top half of the plate then a point located slightly left of mode $(N+1)$ gives larger stress in the bottom half of the plate. Experimental results verified the theoretical predictions.

Acknowledgements

Funding for this research was partially provided by NSF grants CMS-9523349, MSS-9310528 and a grant from the French Government to the first author for his visit to UTC, France. Authors would like to thank Dr. Ph. Gatignol for his valuable inputs during the course of this research.

References

[1] D.N. Alleyne, P. Cawley, The interaction of lamb waves with defects, IEEE Trans. Ultrason., Ferroelect. Freq. Contr. (1992) 381–396.

[2] M.S. Cacei, W.P. Cacheris, Fitting curves to data, Byte (1984) 340–362.

[3] M. Castaings, B. Hosten, Delta operator technique to improve the Thomson–Haskell-method stability for propagation in multilayered anisotropic absorbing plates, J. Acoust. Soc. Am. 95 (4) (1994) 1931–1941.

[4] D.E. Chimenti, R.W. Martin, Nondestructive evaluation of composite laminates by leaky Lamb waves, Ultrasonics 29 (1991) 13–21.

[5] J.J. Ditri, J.L. Rose, G. Chen, Mode selection criteria for defect detection optimization using lamb waves, in: D.O. Thompson, D.E. Chimenti (Eds.), Review of Progress in Quantitative Nondestructive Evaluation, vol. 11, Plenum Press, New York, 1992, pp. 2109–2115.

[6] W. Huang, S.I. Rokhlin, Y.J. Wang, Analysis of different boundary condition models for study of wave scattering from fiber-matrix interphases, J. Acoust. Soc. Am. 101 (1997) 2031–2042.

[7] M.R. Karim, A.K. Mal, Y. Bar-Cohen, Inversion of leaky Lamb wave data by simplex algorithm, J. Acoust. Soc. Am. 88 (1990) 482–491.

[8] V.K. Kinra, V.R. Iyer, Ultrasonic measurement of the thickness, phase velocity, density or attenuation of a thin viscoelastic plate. Part II: the inverse problem, Ultrasonics 33 (1995) 111–122.

[9] T. Kundu, Inversion of acoustic material signature of layered solids, J. Acoust. Soc. Am. 91 (1992) 591–600.

[10] T. Kundu, J. Bereiter-Hahn, K. Hillmann, Measuring elastic properties of cells by evaluation of scanning acoustic microscopy $V(z)$ values using simplex algorithm, Biophys. J. 59 (1991) 1194–1207.

[11] T. Kundu, K.I. Maslov, Material interface inspection by Lamb waves, Int. J. Solids Struct. 34 (1997) 3885–3901.

[12] T. Kundu, K. Maslov, P. Karpur, T. Matikas, P. Nicolaou, A Lamb wave scanning approach for mapping defects in [0/90] titanium matrix composites, Ultrasonics 34 (1996) 43–49.

[13] A.K. Mal, C.C. Yin, Y. Bar-Cohen, Ultrasonic nondestructive evaluation of cracked composite laminate, Compos. Engng. 1 (1991) 85–101.

[14] K.I. Maslov, T. Kundu, Selection of Lamb modes for detecting internal defects in composite laminates, Ultrasonics 35 (1997) 141–150.

[15] P.B. Nagy, L. Adler, D. Mih, W. Sheppard, Single mode Lamb wave inspection of composite laminates, in: D.O. Thompson, D.E. Chimenti (Eds.), Review of Progress in Quantitative NDE, vol. 8B, Plenum Press, New York, 1989, pp. 1535–1542.

[16] A.H. Nayfeh, Wave Propagation in Layered Anisotropic Media, Elsevier, Amsterdam, 1995.

[17] J.A. Nelder, R. Mead, A simplex method for function minimization, Comput. J. 7 (1965) 308–315.

[18] C. Potel, J.F. de Belleval, Propagation in an anisotropic periodically multilayered medium, J. Acoust. Soc. Am. 93 (1993) 2669–2677.

[19] C. Potel, J.F. de Belleval, Acoustic propagation in anisotropic periodically multilayered media: a method to solve numerical instabilities, J. Appl. Phys. 74 (1993) 2208–2214.

[20] T.W. Taylor, A.H. Nayfeh, Dynamic internal response of fluid-loaded multilayered anisotropic media, J. Acoust. Soc. Am. 91 (1992) 2519–2528.

[21] R.-B. Yang, A.K. Mal, Elastic waves in a composite containing inhomogeneous fibers, Int. J. Engng. Sci. 34 (1996) 67–79.

[22] W. Yang, T. Kundu, Guided waves in multilayered anisotropic plates and its use in internal defect detection, ASCE J. Engng. Mech. 124 (1998) 311–318.